CHEMISTRY OF MATERIALS

ARTICLE

pubs.acs.org/cm

Core-Expanded Naphthalene Diimides Fused with Sulfur Heterocycles and End-Capped with Electron-Withdrawing Groups for Air-Stable Solution-Processed n-Channel Organic Thin Film Transistors

Yunbin Hu,[†] Xike Gao,[*,†] Chong-an Di,[*,‡] Xiaodi Yang,[§] Feng Zhang,[†] Yunqi Liu,[‡] Hongxiang Li,[†] and Daoben Zhu[*,‡,†]

[†]Laboratory of Materials Science, Shanghai Institute of Organic Chemistry, Chinese Academy of Sciences (CAS), 345 Lingling Road, Shanghai 200032, China

[‡]Beijing National Laboratory for Molecular Sciences, Key Laboratory of Organic Solids, Institute of Chemistry, Chinese Academy of Sciences (CAS), Beijing 100190, China

[§]Laboratory of Advanced Materials, Fudan University, Shanghai 200433, China

Supporting Information

ABSTRACT: Four families of core-expanded naphthalene diimide (NDI) derivatives were designed and synthesized, namely, NDI-DTYM2 (**1**−**7**, of which **1** and **2** were previously reported), NDI-DTDCN2 (**8** and **9**), NDI-DTYCA2 (**10** and **11**), and NDI-DCT2 (**12**), where the NDI core fuses two 2-(1,3-dithiol-2-ylidene)malonitrile (DTYM) groups, two 1,4-dithiine-2,3-dicarbonitrile (DTDCN) groups, two alkyl 2-(1,3-dithiol-2-ylidene)cyanoacetate (DTYCA) groups, and two 2,3-dicyanothiophenes (DCT), respectively. The NDI cores of the present compounds bear the branched N-alkyl substituents with the carbon atom numbers from 12 to 24, which guarantees good material solubility. The solution-processed, bottom-gate organic thin film transistors based on new compounds **3**−**12** operate well in air with the electron mobility ranging from ~10^{-6} to 0.26 $cm^2 V^{-1} s^{-1}$, depending on the nature of the branched N-alkyl substituent and the π-backbone structure.

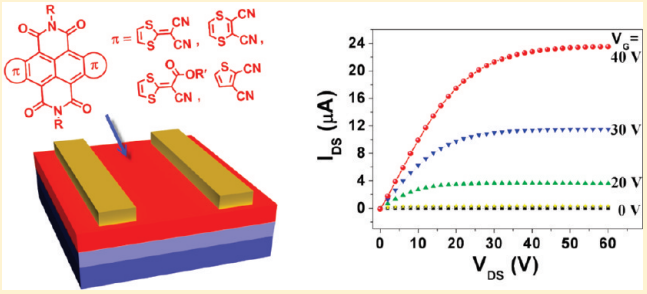

KEYWORDS: characterization of materials, electronic materials, semiconductors

INTRODUCTION

Organic thin film transistors (OTFTs) are attracting ever increasing attention because of their applications for low-cost, large-area, and flexible electronics.[1] These applications mainly include flexible active-matrix displays, radio frequency identification (RFID) tags, and chemical/biological sensors.[2] Organic semiconductors (OSCs), the π-conjugated organic molecules and polymers, are the key components of OTFTs. Historically, the performance of electron-transporting (n-type) OSCs was outmatched by that of their hole-transporting (p-type) counterparts.[3] This fact has become one of the major challenges confronting the field of OTFTs, because both n- and p-type OSCs with comparable performance are necessary for organic complementary circuits.[4] To realize the low-cost and large-area organic electronics, OSCs should be processed from solution using the techniques such as spin coating, casting, and printing.[1a,5] Some solution-processed p-channel OTFTs have shown hole mobilities ≥ 1.0 $cm^2 V^{-1} s^{-1}$ with good air stability,[6] while most of solution-processed n-channel OTFTs exhibit low electron mobilities (μ_e < 0.1 $cm^2 V^{-1} s^{-1}$) and/or less air stability.[7]

Chart 1 summarizes the representative n-type OSCs developed for air-stable solution-processed OTFTs. Katz et al.[8] first reported solution-processed, ambient-stable, n-channel OTFTs based on a fluorocarbon-functionalized naphthalene diimides (NDIs) derivative (Chart 1, NDIF) with μ_e > 0.01 $cm^2 V^{-1} s^{-1}$. Since the R^F groups depress the LUMO energy of NDIF slightly ($\Delta E \leq 0.15$ eV), it was proposed that a kinetic barrier formed by the densely packed R^F groups could hinder the penetration of ambient species (O_2, H_2O) and contribute to the electron-transporting air stability.[8,9] Besides NDIs,[8−10] this fluorocarbon-based air barrier mechanism was also successfully applied to perylene diimides (PDIs),[11] pyromellitic diimides,[12] and other n-type molecules,[13] affording many high performance, air-stable, n-type OSCs with μ_e > 1.0 $cm^2 V^{-1} s^{-1}$ for their vacuum deposited OTFT devices.[10c,11c] Unfortunately, most fluorocarbon-functionalized n-type OSCs suffer from a low solubility in common

Received: October 1, 2010
Revised: December 31, 2010
Published: January 20, 2011

Chart 1. Representative n-Type Organic Semiconductors Developed for Air-Stable Solution-Processed Organic Thin Film Transistors

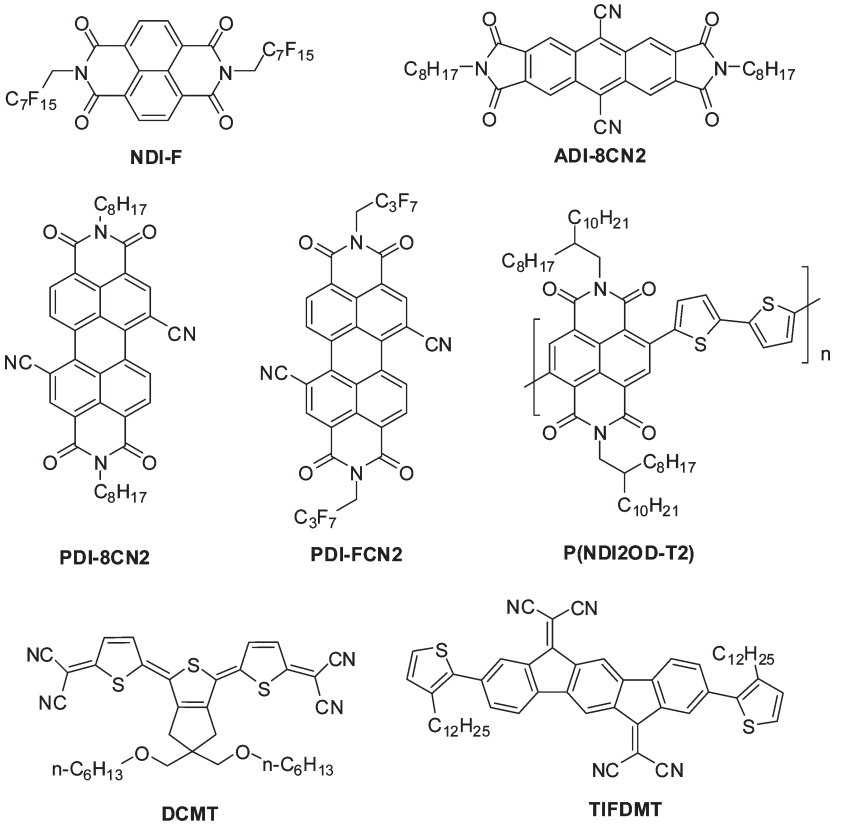

organic solvents,[8−13] which hinders their applications for solution-processed OTFTs. Later on, some core-cyanated arylene diimides (Chart 1, ADI-CN2,[14] PDI-8CN2,[15] and PDI-FCN2[16]) were successfully used for air-stable solution-processed OTFTs, showing electron mobility of 0.01−0.1 $cm^2 V^{-1} s^{-1}$ in ambient. The air stability of these core-cyanated arylene diimides is attributed to their low-lying LUMO levels (approximately −4.1 to −4.5 eV) that can thermodynamically resist electron carrier trapping under ambient conditions.[14,17] A solution-processed DCMT derivative (Chart 1) was reported to exhibit a high electron mobility of up to 0.16 $cm^2 V^{-1} s^{-1}$ in ambient, although its OTFT device suffered from less air stability with the electron mobility dropping to ∼0.01 $cm^2 V^{-1} s^{-1}$ over two months.[18] A ladder-type donor−acceptor (D−A) molecule (Chart 1, TIFDMT) was explored for solution-processed OTFTs, affording an electron mobility as high as 0.16 $cm^2 V^{-1} s^{-1}$ with good air stability.[19] More recently, a high-mobility electron-transporting D−A polymer (Chart 1, P(NDI2OD-T2)), containing NDI and bithiophene repeat units, was reported by Facchetti and coworkers.[20] When this polymer was used for solution fabrication of top-gate OTFTs, the devices exhibited a high electron mobility of up to 0.85 $cm^2 V^{-1} s^{-1}$ in ambient.[20a] However, when P(NDI2OD-T2) was utilized for bottom-gate OTFTs, the devices showed a relative lower electron mobility of 0.06 $cm^2 V^{-1} s^{-1}$ with unsatisfactory air stability, due to the relative high LUMO level of P(NDI2OD-T2) (−3.9 eV).[20b] Therefore, the area of solution-processed n-type OSCs involves not only maximizing the electron mobility of these materials but also minimizing the deterioration of the electronic properties over time when the materials are exposed to ambient.

To develop innovative materials that can surpass the limitations of existing n-type OSCs, effective material-design strategies should be devised, which not only integrate the virtues of the existing n-type OSCs but also can be endowed with new elements.[3,17,21] On the basis of our previous work,[22] we present here in detail a possible molecular design strategy for synthesizing air-stable, solution-processed, n-type OSCs, which benefits from Yamashita et al.'s pioneering work.[23] That is, first select an electron-deficient NDI core that attaches the long, branched N-alkyl chains to ensure good solubility, then fuse the sulfur heterocycles (such as 1,3-dithiol rings, thiophene, etc.) to the NDI core, and finally use the electron-withdrawing groups (such as CN) for the end-capping of the sulfur heterocyles, affording an A−D−A−D−A π-conjugated structure. There are several reasons for this molecular design: (i) the expanded π-conjugation promotes intermolecular $\pi-\pi$ stacking and/or S···S interactions, which is crucial for obtaining high electron mobility; (ii) the end-capped electron-withdrawing group can depress molecular LUMO energies, which is important for realizing electron carrier injection and conduction with ambient stability; (iii) the long, branched N-alkyl chain and the expanded π-conjugation could enable a balance of good solubility, close and efficient $\pi-\pi$ stacking in solid state, excellent crystallinity, and good film formation.

We previously communicated two core-expanded naphthalene diimides fused with 2-(1,3-dithiol-2-ylidene)malonitrile (DTYM)

dx.doi.org/10.1021/cm102850j |*Chem. Mater.* 2011, 23, 1204–1215

groups (Scheme 1, **1** and **2**, R = 2-decyltetradecyl ($C_{14,10}$) and 2-octyldodecyl ($C_{12,8}$), respectively).[22] Here, we name them NDI-DTYM2. The NDI-DTYM2 derivatives **1** and **2** have good solubility in common organic solvents, and their solution-processed Ag-contact OTFTs exhibit a high electron mobility of up to 0.51 $cm^2 V^{-1} s^{-1}$ in ambient.[22]

In the previous work, we found that the structure of the 2-branched N-alkyl chains of **1** and **2** influences their device performance.[22] Moreover, several groups' studies have also demonstrated that the geometry of the side alkyl groups of π-conjugated materials influences their self-assembling behaviors, solid-state morphology control, and resulting device performance.[24] In this contribution, the modification of the branched N-alkyl chains of NDI-DTYM2 derivatives is first studied for elucidating the influence of the N-substituent structure on the device performance. Regulation of the branched N-alkyl chains' structure regarding the length (carbon atom number) and the distance of the branching point from the π-core was performed, affording five new NDI-DTYM2 derivatives (Scheme 1, **3**−**7**). Compounds **3**−**5** attach the 2-branched N-alkyl chains of $C_{10,6}$, $C_{8,6}$, and $C_{8,4}$, respectively. Compounds **6** and **7** possess the 3- and 4-branched N-alkyl substituents of $C_{11,6}$ and $C_{12,6}$, respectively. In addition, three new categories of core-expanded naphthalene diimides (Scheme 1, **8**−**12**), which bear the 2-branched N-alkyl chains of $C_{14,10}$ or $C_{12,8}$, were synthesized and characterized to study the influence of π-conjugated backbone structure on device performance. They are NDI-DTDCN2 (**8** and **9**), NDI-DTYCA2 (**10** and **11**), and NDI-DCT2 (**12**), where the NDI core fuses two 1,4-dithiine-2,3-dicarbonitrile (DTDCN) groups, two alkyl 2-(1,3-dithiol-2-ylidene)cyanoacetate (DTYCA) groups, and two 2,3-dicyanothiophenes (DCT), respectively. Compounds **3**−**12** were studied for solution-processed OTFTs, and all devices perform well in air as n-channel transistors.

RESULTS

Synthesis. A series of core-expanded naphthalene diimides fused with sulfur heterocycles and end-capped with electron-withdrawing groups (**1**−**12**) were synthesized according to Scheme 1. In a recent preliminary communication, we described the syntheses of compounds **1**, **2**, **13**, and **14**.[22] Tetrabromonaphthalene diimides (TBNDIs) **15**−**19**, the key precursors, were synthesized by a dehydrohalogenation-based imidization reaction of tetrabromonaphthalene dianhydride (TBNDA) with the corresponding alkyl amides, as previous reported.[25] NDI-DTYM2 derivatives **3**−**7** were readily prepared in 47−68% yields by the nucleophilic aromatic substitution (S_NAr) reaction of corresponding TBNDIs (**15**−**19**) and sodium 2,2-dicyanoethene-1,1-dithiolate. Accordingly, the S_NAr reaction of TBNDIs (**13** and **14**) and sodium 1,2-dicyanoethene-1,2-dithiolate afforded NDI-DTDCN2 derivatives **8** and **9**, with the yield of 40% and 35%, respectively. The reaction of alkyl (ethyl or hexyl) 2-cyanoacetate, NaH, and CS_2 in dry THF gave corresponding sodium 2-cyano-3-alkyloxy-3-oxoprop-1-ene-1,1-dithiolate, which was not isolated and then used for the S_NAr reaction with **14**, affording NDI-DTYCA2 derivatives **10** and **11** in 73% and 47% yield, respectively. The simple ^1H NMR and ^{13}C NMR spectra of **10** and **11** imply that there is no cis−trans isomerism and their molecules are probably energy optimized trans isomers. According to a modified method of the preparation of dinaphtho[2,3-*b*:2′,3′-*d*]thiophene-5,7,12,13-tetrone,[26] NDI-DCT2 derivative **12**, as an inseparable mixture of syn and anti isomers, was achieved in

Scheme 1. Synthesis of Core-Expended Naphthalene Diimides Derivatives (1−12)[a]

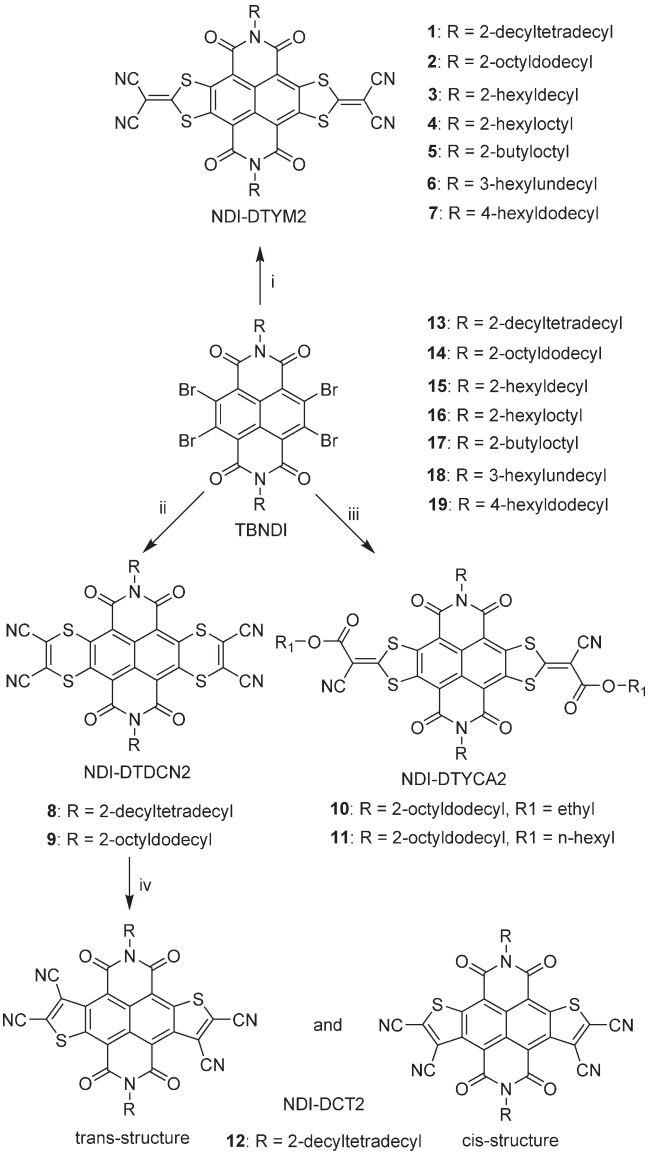

[a] (i) Sodium 1,1-dicyanoethene-2,2-dithiolate, THF, 50 °C. (ii) Sodium 1,2-dicyanoethene-1,2-dithiolate, THF, 30 °C. (iii) NaH, ethyl 2-cyanoacetate or hexyl 2-cyanoacetate, THF, 0−5 °C; CS_2, room temperature. (iv) H_2O_2 (30%), C_2H_5COOH, 120 °C.

30% yield by the oxidation of **8** with hydrogen peroxide in propionic acid. The syn−anti isomerism of **12** is revealed by the ^{13}C NMR spectra analysis, where more carbon signals appear in the aromatic region than those of either a syn or anti structure, indicating an overlap of their carbon signals. This syn−anti isomerism is also existent for acenedithiophene derivatives.[27] Compounds **3**−**12** were characterized by ^1H- and ^{13}C NMR spectra, elemental analysis, mass spectroscopy (MALDI-TOF), and IR spectra. Compounds **1**−**12** are highly soluble in common organic solvents such as $CHCl_3$, CH_2Cl_2, and THF, which makes it possible to fabricate their OTFT devices by conveniently using the solution-based techniques.

DFT Calculations. Using the Gaussian 03 program at the B3LYP/6-31G(d) level, density functional theory (DFT)

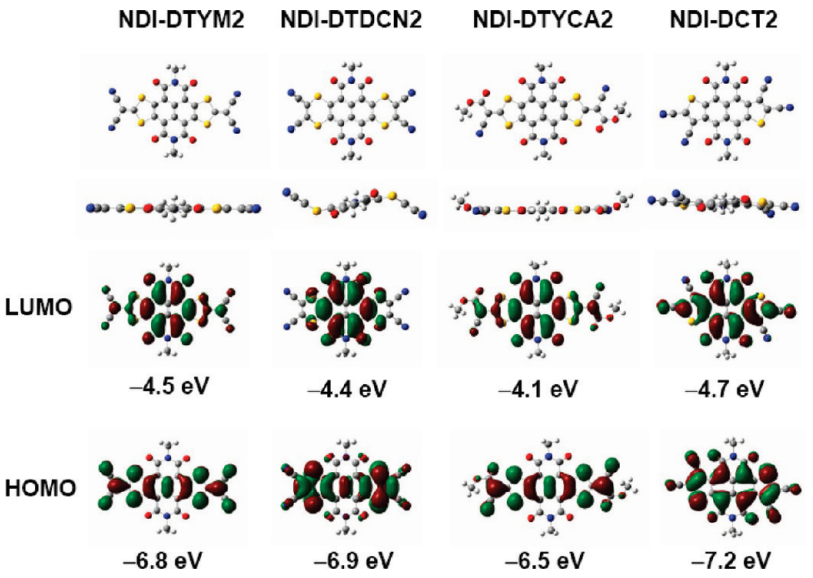

Figure 1. The geometries, frontier orbitals, and MO energies of model molecules for NDI-DTYM2, NDI-DTDCN2, NDI-DTYCA2, and NDI-DCT2 derivatives, obtained by DFT calculations.

calculations were previously performed for evaluating the position and energies of frontier obtitals for NDI-DTYM2 derivatives (**1** and **2**).[22] The electron density distribution and energies of frontier orbitals for NDI-DTDCN2, NDI-DTYCA2, and NDI-DCT2 derivatives were estimated by the same DFT calculations, where all alkyl chains were replaced by methyl groups to reduce the time required for calculation. The substitution of alkyl chain with methyl group should not affect the calculations because the influence of alkyl chains on the electron structure of the molecule is considered negligible. Figure 1 shows the DFT-calculated geometries, frontier obtitals, and molecular orbitals (MO) energies of model molecules for NDI-DTYM2 (**1**−**7**), NDI-DTDCN2 (**8** and **9**), NDI-DTYCA2 (**10** and **11**), and NDI-DCT2 (**12**). The model molecules of NDI-DTYM2 and NDI-DTYCA2 have the rigid and entirely coplanar π-conjugated backbones, and the π-conjugation of NDI-DCT2 is generally coplanar with slight atom deviations, while the model molecule of NDI-DTDCN2 possesses a bended π-conjugated skeleton with a dihedral angle of about 130° between the maleonitrile moiety and NDI core. The electron density distribution of frontier orbitals for NDI-DTDCN2 (**8** and **9**) and NDI-DTYCA2 (**10** and **11**) is similar to that for NDI-DTYM2 (**1**−**7**), where the largest coefficients in the HOMO orbitals are located on the long axis of the π-systems, and the coefficients in the LUMO orbitals are mainly positioned on the central NDI units. The results indicate that there might be considerable intramolecular charge transfer. For NDI-DCT2 (**12**), the electron density of the HOMO orbital is distributed across the full π-conjugated backbone, and that of the LUMO orbital is located on most of the π-conjugation with little or no density on sulfur atoms and partial cyano groups, demonstrating the weak intramolecular charge transfer. The model molecule of NDI-DTYM2 is isomeric with that of NDI-DTDCN2, and they share the comparable HOMO/LUMO energies (−6.8/−4.5 versus −6.9/−4.4 eV). NDI-DTYCA2 derivatives can be regarded as the products achieved by the replacement of two centrosymmetric cyano groups of NDI-DTYM2 derivatives with two alkyl ester moieties. This molecular structure change does affect the molecular orbital energies, both HOMO and LUMO energies of NDI-DTYCA2 shift upward versus those of NDI-DTYM2 (−6.8/−4.5 eV), affording relatively higher HOMO/LUMO energies (−6.5/−4.1 eV). This upward-shift of MO energies can be explained by the weaker electron-withdrawing ability of the alkyl ester moiety versus that of the cyano group.[7c] NDI-DCT2 presents the lowest HOMO/LUMO energies (−7.2/−4.7 eV) with a band gap of 2.5 eV, indicating the strong electron deficiency. It should be noted that the anti and syn isomers of NDI-DCT2 have similar electron density distribution of MO orbitals (Figure 1 and Supporting Information Figure S1) and almost equivalent HOMO/LUMO energies (−7.20/−4.70 eV versus −7.21/−4.66 eV). This negligible energy difference between anti and syn isomers was also found in the p-type anthradithiophene system.[28]

Thermal Properties. Thermogravimetric analysis (TGA) and differential scanning calorimetry (DSC) were carried out under nitrogen atmosphere to evaluate the thermal behaviors of semiconductors **3**−**12**. The onset decomposition temperatures (T_d) estimated by TGA and the phase transition temperature (T_{pt}) obtained by DSC are collected in Table 1. The representative TGA and DSC plots of **3**−**12** are shown in Figure 2 and in Supporting Information Figures S2−S6. The T_d values of the present materials are in the following order: 370−389 °C for NDI-DTYM2 (**3**−**7**) that are comparable to those of **1** and **2** (both at 386 °C)[22] > 344−350 °C for NDI-DTYCA2 (**10** and **11**) and NDI-DCT2 (**12**) > 284−290 °C for NDI-DTDCN2 (**8** and **9**). Similar to the thermal behavior of **1** and **2**,[22] compounds **3**, **7**, and **10** showed no phase transition signals before melting in the second heating−cooling DSC cycles (Supporting Information Figure S2). As shown in Supporting Information Figures S3 and S4, compounds **4**−**6**, **8**, and **9** all presented a couple of reversible endothermic and exothermic peaks before melting in repeated heating−cooling DSC cycles, and their T_{pt} values are in a decreased order (see Table 1 for details). Compound **11** displayed quasi-reversible endothermic (193/238 °C) and exothermic (173/227 °C) peaks in repeated heating−cooling DSC cycles (Supporting Information Figure S5). As shown in Supporting Information Figure S6, there is only a melting/crystallizing

dx.doi.org/10.1021/cm102850j |*Chem. Mater.* 2011, 23, 1204–1215

Table 1. Thermal, Optical, and Electrochemical Data for Semiconductors 3−12

	T_{pt}[a] (°C)heating (cooling)	T_d[b] (°C)	λ_{max}^{sol} (nm) (E_g/eV)[c]	$\lambda_{max}^{thin\text{-}film}$ (nm) (E_g/eV)[d]	$E_{red1}^{1/2}$ (V)[e]	$E_{red2}^{1/2}$ (V)[e]	LUMO (eV)[f]	HOMO (eV)[g]
3	N.A. (N.A.)	370	573 (2.1)	594 (2.0)	−0.09	−0.63	−4.35	−6.45
4	208 (184)	389	573 (2.1)	601 (2.0)	−0.08	−0.64	−4.36	−6.46
5	172 (158)	388	573 (2.1)	602 (2.0)	−0.08	−0.63	−4.36	−6.45
6	145 (115)	372	572 (2.1)	601 (2.0)	−0.06	−0.54	−4.38	−6.46
7	N.A. (N.A.)	384	572 (2.1)	603 (2.0)	−0.08	−0.61	−4.36	−6.44
8	91, 238, (85, 231)	290	551 (2.0)	542 (2.1)	−0.16	−0.65	−4.28	−6.28
9	89 (82)	284	550 (2.0)	540 (2.1)	−0.16	−0.64	−4.28	−6.28
10	N.A. (N.A.)	347	581 (2.0)	595 (1.9)	−0.21	−0.66	−4.23	−6.23
11	193, 238 (173, 227)	344	582 (2.0)	594 (2.0)	−0.21	−0.68	−4.23	−6.23
12	158 (138, 129)	350	545 (2.2)	540[h] (2.1)	0.19	−0.39	−4.63	−6.83

[a] Phase transition temperature obtained from DSC scans of the second heating−cooling cycle under nitrogen at a scan rate of 10 °C/min. [b] Onset decomposition temperature measured by TGA under a nitrogen flow at a temperature ramp of 10 °C/min. [c] The maximum end absorption wavelength of the UV−vis spectrum in CH_2Cl_2, optical band gap (E_g) is estimated from the edge of end absorption. [d] The maximum end absorption wavelength of the UV−vis spectrum as drop-casted thin film on glass, optical band gap (E_g) is estimated from the edge of end absorption. [e] 0.1 M $[Bu_4N]PF_6$ in CH_2Cl_2 (vs SCE) at a scan rate of 50 mV/s. [f] Estimated from the equation LUMO = $-4.44 - E_{red1}^{1/2}$. [g] Estimated from HOMO = LUMO − E_g. [h] This maximum wavelength is calculated from the central peak of a broad end absorption that contains three shoulder peaks.

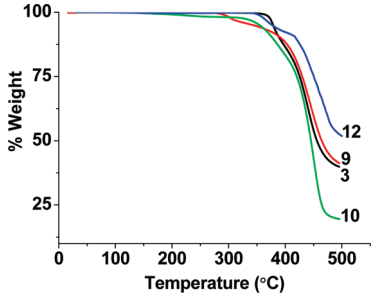

Figure 2. TGA plots of compounds **3**, **9**, **10**, and **12** with a heating rate of 10 °C/min under a nitrogen flow.

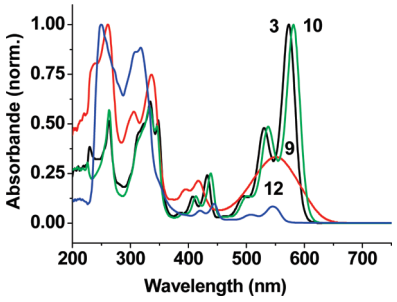

Figure 3. Optical absorption spectra of compounds **3**, **9**, **10**, and **12** in CH_2Cl_2 solutions.

transition in the heating−cooling DSC scans of **12**. The melting peak of **12** (158 °C) is strong and sharp, but its crystallizing peak is broad and can be divided into a main peak (138 °C) and a shoulder peak (129 °C), which might be explained by **12** being a mixture of syn and anti isomers. By and large, the general reversibility of DSC scans of **3**−**12** and their relatively high T_d values (284−389 °C) are clear indications of their good thermal stability. In addition, conventional melting point determinations were performed on compounds **3**−**12**, of which **12** possesses the lowest melting point value (about 160 °C versus 158 °C by DSC). Semiconductors **3**−**11** exhibited relatively higher melting points (≥239 °C versus 238 °C by DSC), which together with their relatively high T_d values (>280 °C) allows thin film crystallinity and microstructure analysis over a broad range of annealing temperatures, from room temperature to about 200 °C.

Optical and Electrochemical Properties. UV−vis absorption spectra and cyclic voltammetry measurements were conducted to investigate optical and electrochemical properties of semiconductors **3**−**12**. The optical and electrochemical data are summarized in Table 1. Figure 3 and Supporting Information Figure S7 exhibit the representative UV−vis spectra in dichloromethane solution and in thin films, respectively. Solution and solid state optical band gaps (E_g^{opt}) were determined from the edges of end absorptions of the UV−vis spectra. Compounds **3**−**12** have comparable optical band gaps of 2.0−2.2 eV in solution and 1.9−2.1 eV in thin film, which are consistent with the DFT-calculated values (2.3−2.5 eV) with a slight derivation of 0.3−0.4 eV. The same series of semiconductors showed nearly identical absorption spectra in dichloromethane with the nearly identical peak values for their end absorptions (see Table 1 for details), indicating that optical properties are insensitive to the structure of the N-alkyl chain as expected. NDI-DTYM2 (**3**) and NDI-DTYCA2 (**10**) have comparable energy gaps (2.1 versus 2.0 eV) and display almost identical peak shape with a slight peak shift (8 nm) for the end absorptions (Figure 3). The results demonstrate that NDI-DTYM2 and NDI-DTYCA2 have the similar molecular electronic structure, which has been confirmed by the above DFT calculations, where they possess identical electron density distribution of MO orbitals and comparable theoretical band gaps (2.3 versus 2.4 eV). NDI-DCT2 (**12**) exhibited the weakest absorptions at low energy band (Figure 3), demonstrating the weak intramolecular charge transfer, as evidenced by DFT results.

A comparison of the end absorption in as-deposited thin film and that in solution shows that NDI-DTYM2 (**3**−**7**) presented larger red shifts (about 21−31 nm) than those of NDI-DTYCA2 (**10** and **11**, 14 and 12 nm, respectively), whereas NDI-DTDCN2 (**8** and **9**) and NDI-DCT2 (**12**) exhibited blue shifts of 9, 10, and 5 nm, respectively. The blue-shift behaviors of **8**, **9**, and **12** are probably due to the formation of H-type molecular aggregation in thin film.

To evaluate the changes of molecular arrangement in thin film upon annealing, UV−vis studies were performed on the thin films of the representative NDI-DTYM2 derivatives **3**, **6**, and **7**,

dx.doi.org/10.1021/cm102850j |*Chem. Mater.* 2011, 23, 1204–1215

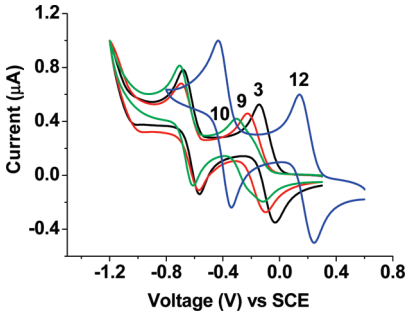

Figure 4. Cyclic voltammograms of compounds **3**, **9**, **10**, and **12** (10^{-3} mol L^{-1}) with 0.1 mol L^{-1} Bu_4NPF_6 in CH_2Cl_2 solutions and scan rate of 50 mV s^{-1}.

which possess the 2-, 3-, and 4-branched N-alkyl chains of $C_{10,6}$, $C_{11,6}$, and $C_{12,6}$, respectively, with the comparable carbon atom numbers of 16−18. As shown in Supporting Information Figures S8−S10, when the thin films were annealed at 120, 160, and 180 °C, **3** and **6** showed slightly red shifts of 2−5 nm in comparison with their as-deposited films, while thin films of **7** exhibited a large blue shift of 18 nm relative to the as-deposited films. The remarkable blue-shift behaviors of thin films of **7** upon annealing demonstrate that the molecular packing is greatly changed when annealed at 120 °C and keeps almost unchanged at higher annealing temperatures.

Figure 4 shows the representative cyclic voltammograms. All semiconductors display two reversible reduction processes in dichloromethane solution. The first and second half-wave reductive potentials ($E_{red1}^{1/2}$ and $E_{red2}^{1/2}$) were extracted as the midpoints between the peak potentials of the forward and reverse scans. NDI-DTYM2 (**3**−**7**) exhibited nearly identical redox features, with $E_{red1}^{1/2}$ at about −0.08 V (vs SCE). The values of $E_{red1}^{1/2}$ for NDI-DTDCN2 (**8** and **9**) are about −0.16 V, where there is about a 0.08 V cathodic shift with respect to those of **3**−**7**, suggesting less electron affinity of NDI-DTDCN2 versus NDI-DTYM2. NDI-DTYCA2 (**10** and **11**) have more negative $E_{red1}^{1/2}$ values (about −0.21 eV) than those of NDI-DTYM2 (**3**−**7**). The less electron-withdrawing ability of the alkyl ester moiety relative to the cyano group explains the cathodic shift of $E_{red1}^{1/2}$ (about 0.13 V) of NDI-DTYCA2 versus that of NDI-DTYM2.[7c] For NDI-DCT2 (**12**), $E_{red1}^{1/2}$ = 0.19 V, which is even more positive than that of TCNQ (about 0.17 V vs SCE) measured under the same conditions, indicating the strong electron-accepting property.

From $E_{red1}^{1/2}$ values, LUMO energies for the present semiconductors can be estimated by taking the SCE energy level to be −4.44 eV below the vacuum level and using the formula LUMO = −4.44 eV − $E_{red1}^{1/2}$.[29] Accordingly, HOMO energies were evaluated using standard approximations by the formula HOMO = LUMO − E_g^{opt}. All semiconductors showed low-lying LUMO levels (<−4.2 eV), with the energy values (eV) in the following order: −4.63 for NDI-DCT2 (**12**) < −4.35 ∼ −4.38 for NDI-DTYM2 (**3**−**7**) < −4.28 for NDI-DTDCN2 (**8** and **9**) < −4.23 for NDI-DTYCA2 (**10** and **11**), which are consistent with the DFT-calculated values ranging from −4.7 to −4.1 eV in the same order. The experimental and theoretical HOMO energies for the present materials are more negative than −6.2 and −6.5 eV, respectively. Therefore, compounds **3**−**12** are typical n-channel organic semiconductors with the low-lying LUMO energies (<−4.2 eV) that can thermodynamically resist electron carrier trapping under ambient conditions.[14,17,19,30] The stable LUMO energy and the good solubility make semiconductors **3**−**12** promising candidates for solution-processed, ambient-stable, n-channel organic thin film transistors.

Thin-Film Morphologies. X-ray diffraction (XRD) and atomic force microscopy (AFM) were utilized to investigate the thin film microstructures. Measurements were carried out on spin-coated thin films (40−60 nm in thickness) deposited on octadecyltrichlorosilane (OTS)-treated Si/SiO_2 substrates. Figure 5 shows the XRD patterns of thin films of representative compounds (**3**, **4**, and **9**−**12**). Thin films of NDI-DTYM2 (**3**−**6**) and NDI-DTDCN2 (**9**) exhibited intense and sharp Bragg reflections up to third, fourth, or higher order (see Figure 5a−c and Supporting Information Figures S11 and S12), indicating high degree of crystallinity. However, the thin film of NDI-DTYM2 (**7**) showed relatively lower diffraction intensity, and there is a lack of progressive Bragg reflections (Supporting Information Figure S13), implying a less-ordered microstructure. In addition, the film microstructures appeared more complex for **3**−**5**, especially for **5** (Supporting Information Figure S11) where at least two families of diffraction features were obviously observed, manifesting the existence of different phases/orientations in the thin films.[17] As shown in Figure 5d,e, thin films of NDI-DTYCA2 (**10** and **11**) showed much lower diffraction intensity, fewer progressions of Bragg reflections, and larger full width at half-maximum (fwhm) values in comparison with those of thin films of **3**−**6** and **9**, demonstrating less crystallinity. As displayed in Figure 5f, sharp reflections with narrow fwhm values were observed for the thin film of NDI-DCT2 (**12**), implying good crystallinity.

Figure 6 (a−o) shows representative AFM images of spin-coated thin films of **3**−**5**, **9**, and **11** annealed at different temperatures. Along with annealing temperature ranging from 120 to 180 °C, visible changes of thin film morphology were found for each compound. Besides the smooth, continuous, and crystalline film morphology features, NDI-DTYM2 (**3**−**5**) presented the similar film morphology variations upon annealing, that is, the grain size increased (the average grain size values: 250/500/300 nm at 120 °C; 450/700/400 nm at 160 °C; 1000/1500/800 nm at 180 °C for **3**−**5**, respectively) and the grain boundaries decreased (Figure 6a−i). It should be noted that the thin films of **4** exhibited larger average grain size values than those of thin films of **3** and **5** at each annealing temperature (Figure 6a−i), indicating the better crystallinity of **4** than that of **3** and **5**. The different crystallinity might be ascribed to the different symmetrical properties of 2-branched N-alkyl chains (the symmetrical 2-C_6C_6 for **4** versus the asymmetrical 2-C_8C_6 and 2-C_6C_4 for **3** and **5**, respectively). When annealed at 120 and 160 °C, thin films of **6** exhibited generally continuous morphology with large grain sizes (Supporting Information Figure S14a,b). However, upon annealing at 180 °C, the film morphology of **6** became less continuous (Supporting Information Figure S14c). Whether annealed at 120, 160, or 180 °C, thin films of **7** all presented the discontinuous morphology (Supporting Information Figure S14d−f). AFM images (Figure 6j−l) reveal smooth, continuous, polycrystalline films of **9**, and its average grain size increased with annealing from 100 nm (120 °C) to 400 nm (160 °C) and 600 nm (180 °C). In comparison with thin-film morphologies of **3**−**5**, **9** appeared less crystalline for the absence of large plate-like grains. When annealed at 120 °C, the thin film of NDI-DTYCA2 (**11**) showed some discontinuous features with distinct cracks (Figure 6m). A crystalline phase transformation was observed for the thin film of **11** when annealed at 160 °C, yielding uniform spherical grains (about 400 nm in size) with a large density of grain

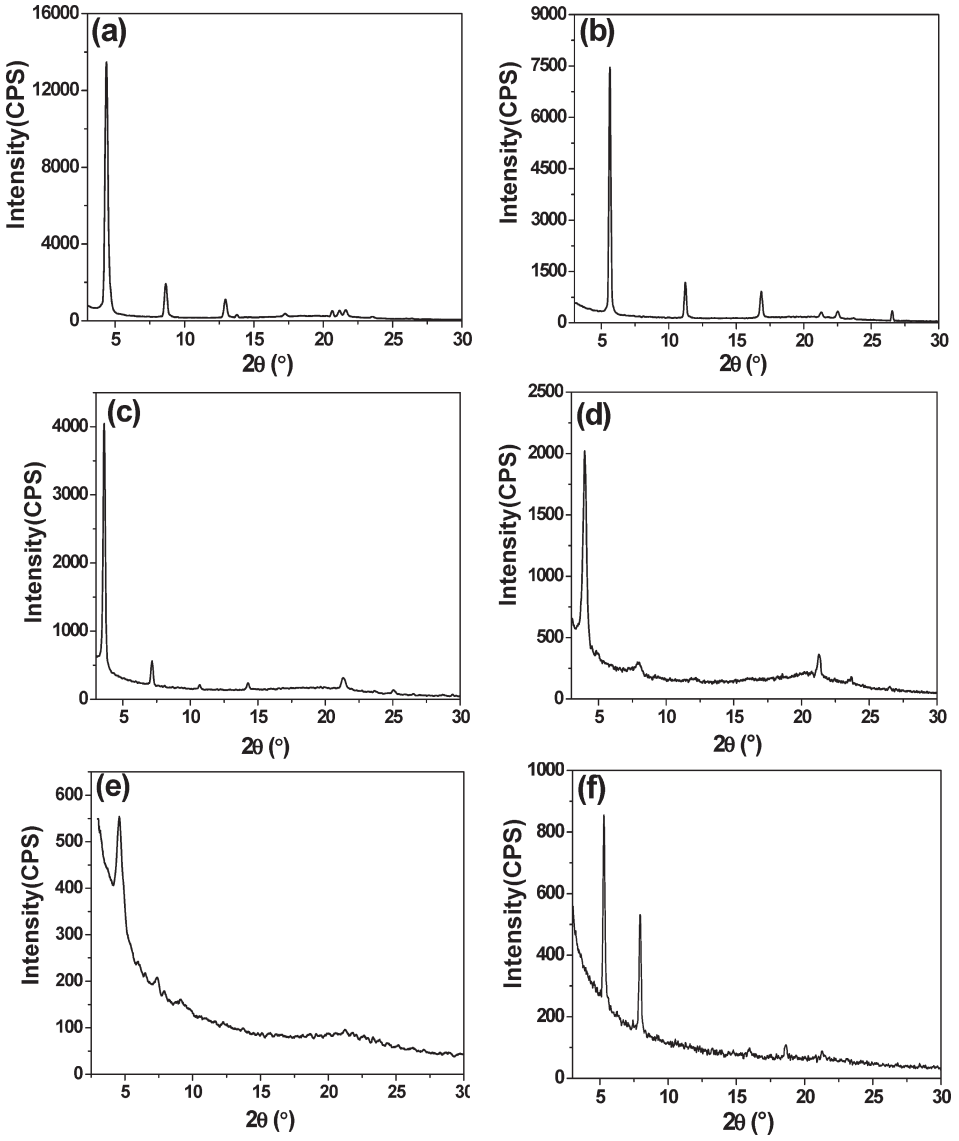

Figure 5. X-ray diffraction patterns of spin-coated thin films of semiconductors **3** (a, annealed at 160 °C), **4** (b, annealed at 160 °C), **9**−**11** (c−e, annealed at 160 °C), and **12** (f, annealed at 120 °C) on OTS-treated SiO_2 substrates.

boundaries (Figure 6n). However, further annealing (at 180 °C) resulted in less improvement for film morphology of **11** (Figure 6o). As shown in Supporting Information Figure S15, thin films of NDI-DTYCA2 (**10**) also exhibited poor discontinuous film morphologies at each annealing temperature. The thin film of **12** (annealed at 120 °C) displayed the generally smooth polycrystalline morphology, but there are a number of circular holes with the depth of 20−30 nm within the film (Supporting Information Figure S16).

Thin Film Transistor Device Characterization. OTFT devices based on **3**−**12** were fabricated by spin-coating methods with a bottom-gate top-contact device configuration (see Supporting Information for details). A minimum of 10 devices for each material were tested under ambient conditions. Thin films of **3**−**12** all displayed positive amplification and performed as air-stable n-channel transistors with well-defined linear and saturation regimes (Figure 7 and Supporting Information Figures S17−S20). The OTFT characteristics of **3**−**12** are summarized in Table 2.

The as-spun (unannealed) thin film devices based on NDI-DTYM2 (**3**−**7**) showed relatively low electron mobilities (μ_e) of about 10^{-3}−10^{-2} $cm^2\ V^{-1}\ s^{-1}$. Similar to previously reported OTFT devices based on **2**,[22] when subjected to annealing temperatures ranging from 120 to 180 °C, the electron mobility of devices based on **3**−**5** showed a stepwise improvement (see Table 2 for details) with the current on/off ratios ($I_{on/off}$) > 10^5 and threshold voltages (V_T) < 15 V. This positive effect is ascribed to the improved thin-film morphology (the increased grain size and the decreased grain boundaries), which was revealed by AFM images (Figure 5a−i). When annealed at 180 °C, thin films of **3**−**5** presented the highest electron mobilities of 0.19−0.21 $cm^2\ V^{-1}\ s^{-1}$. Figure 7a,b displays the output and transfer characteristics of a device based on **3**, with $\mu_e = 0.17\ cm^2\ V^{-1}\ s^{-1}$, $I_{on/off} = 2.8 \times 10^7$, and V_T = 8 V. On the whole, OTFT devices based on **3**−**5** exhibited comparable average μ_e values at each annealing temperature (see Table 2 for details). As shown in Table 2, when annealed at 120 and 160 °C, thin films of **6** exhibited relatively higher average μ_e values than those of devices based on **3**−**5**,

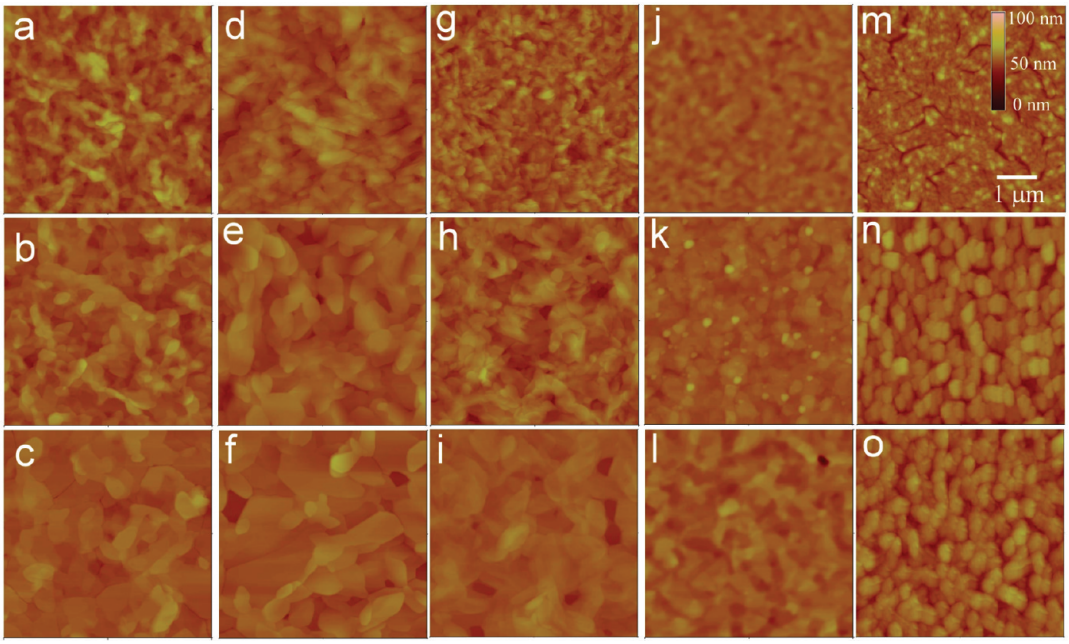

Figure 6. AFM images of thin films of **3** (a−c), **4** (d−f), **5** (g−i), **9** (j−l), and **11** (m−o), where annealing temperatures are 120 (top), 160 (middle), and 180 °C (bottom) from top to bottom.

with the maximum electron mobility of up to 0.26 $cm^2 V^{-1} s^{-1}$ (annealed at 160 °C). Supporting Information Figure S18 exhibits the output and transfer characteristics of an OTFT device based on **6**. However, thin films of **6** annealed at 180 °C showed a lower average electron mobility of 0.18 $cm^2 V^{-1} s^{-1}$ compared with that of thin films annealed at 160 °C (0.24 $cm^2 V^{-1} s^{-1}$) due to the discontinuous film morphology (Supporting Information Figure S14c, annealed at 180 °C). To our surprising, when annealed at 120, 160, and 180 °C, thin films of **7** showed much lower electron mobilities by 2 orders of magnitude (about 10^{-3} $cm^2 V^{-1} s^{-1}$) than those of thin films of **3**−**6**. Moreover, the as-spun thin films of **7** exhibited even higher μ_e values (about 10^{-2} $cm^2 V^{-1} s^{-1}$) versus those of the thin films upon annealing. Supporting Information Figure S19 shows the transfer characteristics of a device based on **7** with the as-deposited film.

The air stability of OTFT devices based on **3** and **4** (annealed at 180 °C) was tested over a period of 75 days in ambient. For a **3**-based device, as shown in Figure 8a, an electron mobility about 0.15 $cm^2 V^{-1} s^{-1}$ maintained nearly unchanged during the first 5 weeks, when the testing time was further delayed to 75 days, the electron mobility could still possess approximately 70% of the pristine value, with a stable on/off current ratio > 10^6. As shown in Supporting Information Figure S21a, a similar air stability was observed for an OTFT device based on **4**, and the electron mobility showed a slight decrease from the pristine value of 0.18 to 0.13 $cm^2 V^{-1} s^{-1}$ during a 75-day test, with a long-term stability for the on/off current ratio (>10^6). Furthermore, the operating stability of OTFT devices based on **3** and **4** was evaluated by using a current on/off switch test in air (Figure 8b and Supporting Information Figure S21b), where there was a very slight current degradation during a 4000-cycle test.

NDI-DTDCN2 derivatives **8** and **9**, which bear the 2-branched $C_{14,10}$ and $C_{12,8}$ N-alkyl chains, respectively, exhibited comparable device performance with electron mobility ranging from 10^{-3} to 10^{-2} $cm^2 V^{-1} s^{-1}$ (see Table 2 for details). Figure 7c,d present the output and transfer characteristics of a device based on **9**, with an electron mobility of 0.016 $cm^2 V^{-1} s^{-1}$, an on/off current ratio of 5.4 × 10^6, and a threshold voltage of 15 V. Compounds **8** and **9** are isomeric compounds of **1** and **2**, respectively. However, OTFT devices based on **8** and **9** showed inferior performance with the maximum electron mobility lower by more than 1 order of magnitude versus that of **1**- and **2**-based devices (0.20 and 0.42 $cm^2 V^{-1} s^{-1}$).[22] In comparison with the device performance of NDI-DTYM2 derivatives **1**−**6**, devices based on NDI-DTYCA2 (**10** and **11**) showed much inferior performance with $\mu_e \leq 4 \times 10^{-3}$ $cm^2 V^{-1} s^{-1}$. Supporting Information Figure S20 exhibits the output and transfer characteristics of an OTFT device based on **10** with μ_e = 0.001 $cm^2 V^{-1} s^{-1}$, I_{on}/I_{off} = 2.4 × 10^4, and V_T = 14 V. OTFT devices based on **12** (annealed at 120 °C) also exhibited low electron mobilities of 10^{-4}−10^{-3} $cm^2 V^{-1} s^{-1}$. The output and transfer characteristics of a **12**-based device are displayed in Figure 7e,f, with μ_e = 0.001 $cm^2 V^{-1} s^{-1}$, I_{on}/I_{off} = 7 × 10^4, and V_T = 8 V.

DISCUSSION

Molecular Electronic Structure vs OTFT Air Stability. OTFT devices based on NDI-DTYM2 (**1**−**7**), NDI-DTDCN2 (**8** and **9**), NDI-DTYCA2 (**10** and **11**), and NDI-DCT2 (**12**) all operate well in air as n-channel transistors. Since thin films of present semiconductors possess diverse morphologies and microstructures as revealed by aforementioned XRD and AFM studies, the device ambient stability is mainly governed by their low-lying LUMO levels (<−4.2 eV), where an onset LUMO level < −4.0 eV is expected to thermodynamically resist electron carrier trapping in ambient.[14,17,19,30] It should be noted that OTFT devices based on NDI-DTYM2 (**1**−**6**) that bear long 2- or 3-branched N-alkyl chains showed excellent operating and storage stability under ambient conditions as evidenced by our previous work[22] and by aforementioned studies (Figure 8 and Supporting Information Figure S21). Up to now, the organic electron charge transport mechanisms and trapping are still not fully understanded.[10d,31] The excellent air and operating stability

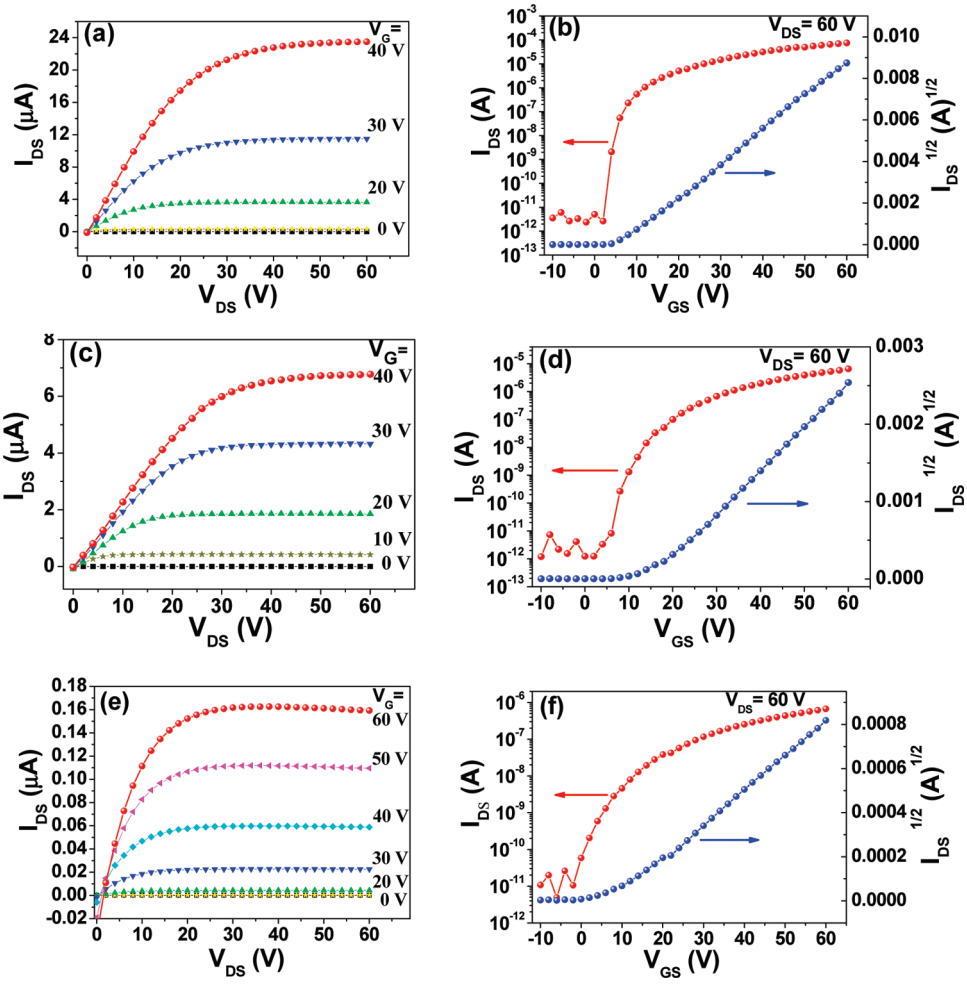

Figure 7. Output and transfer characteristics of OTFT devices based on **3** (a, b), **9** (c, d), and **12** (e, f), respectively, spin coated on OTS-treated SiO_2/Si substrate and annealed at 180 °C (**3** and **9**) or 120 °C (**12**); I_{DS} was obtained at drain-source voltage V_{DS} = 60 V.

Table 2. Maximum (Average) Electron Mobilites (μ_e), Current On/Off Ratios (I_{on}/I_{off}), and Threshold Voltages (V_T) for Thin Films of 3−12 Fabricated by Spin Coating on OTS-Treated Si/SiO_2 Substrates Annealed at 120, 160, and 180 °C

	annealed at 120 °C			annealed at 160 °C			annealed at 180 °C		
	μ_e[a] ($cm^2\ V^{-1}\ s^{-1}$)	I_{on}/I_{off}[a]	V_T[a] (V)	μ_e[a] ($cm^2\ V^{-1}\ s^{-1}$)	I_{on}/I_{off}[a]	V_T[a] (V)	μ_e[a] ($cm^2\ V^{-1}\ s^{-1}$)	I_{on}/I_{off}[a]	V_T[a] (V)
3	0.10 (0.09)	10^5-10^6	2−10	0.14 (0.13)	10^5-10^6	2−10	0.19 (0.17)	10^5-10^6	5−11
4	0.08 (0.07)	10^5-10^6	1−5	0.16 (0.15)	10^5-10^6	3−11	0.21 (0.20)	10^5-10^6	2−10
5	0.12 (0.11)	10^5-10^6	6−3	0.15 (0.14)	10^5-10^6	8−14	0.21 (0.19)	10^6-10^8	7−14
6	0.14 (0.12)	10^6-10^7	−1−5	0.26 (0.24)	10^6-10^7	−1−7	0.20 (0.18)	10^6-10^7	−2−4
7	0.002 (0.001)	10^2-10^3	−10−5	0.004 (0.003)	10^3-10^5	0−5	0.003 (0.002)	10^3-10^4	−4−5
8	0.007 (0.003)	10^3-10^4	8−17	0.016 (0.011)	10^3-10^4	5−10	0.015 (0.008)	10^3-10^4	5−10
9	0.002 (0.001)	10^4-10^5	20−40	0.016 (0.01)	10^4-10^5	10−35	0.007 (0.005)	10^3-10^4	20−41
10	5×10^{-4} (3×10^{-4})	10^3-10^4	32−45	1.1×10^{-3} (9×10^{-4})	10^3-10^4	12−35	4×10^{-3} (2×10^{-3})	10^3-10^4	10−16
11	2×10^{-6}	$10-10^2$	15−20	1.5×10^{-5}	10^2-10^3	10−15	9×10^{-5}	10^2-10^3	3−9
12	1.2×10^{-3} (6×10^{-4})	10^4-10^5	2−11						

[a] Typical device characteristics obtained from about 10 devices, and all devices were measured under ambient conditions.

for devices based on NDI-DTYM2 (**1**−**6**) might be ascribed to the combination of the low-lying LUMO levels (about −4.35 eV), the good crystallinity, and the smooth interconnected thin film morphology with the large plate-like grains and the low density of grain boundaries.[11c,14,17,19,32] In addition, the packing structure of the long, 2-branched N-alkyl chains might protect the π-conjugations against the penetration of ambient species and contribute to the device stability of NDI-DTYM2 derivatives.[33]

Molecular Architecture vs OTFT Performance[34]**.** Figure 9 was used to evaluate the influence of chain length of 2-branched

dx.doi.org/10.1021/cm102850j |*Chem. Mater.* 2011, 23, 1204–1215

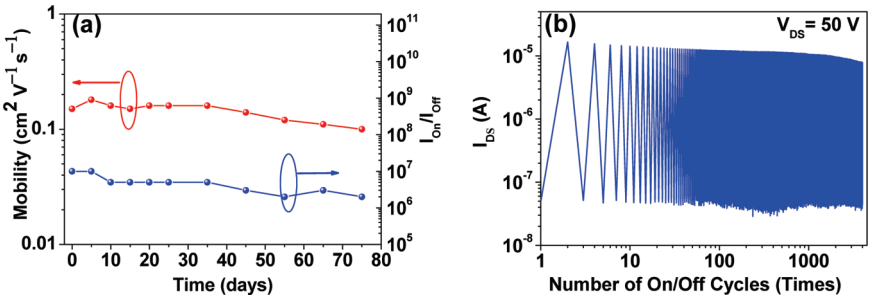

Figure 8. (a) Statistics of mobilities (red) and current on/off ratios (blue) of an OTFT device based on **3** fabricated by spin-coating (annealed at 180 °C) and tested over a period of 75 days in ambient. (b) Electrical characteristics of a **3**-based OTFT during current on/off cycle test (4000 times, V_{GS} = 0 V (off) and 50 V (on)).

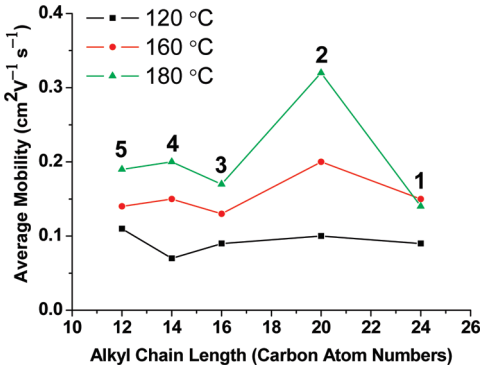

Figure 9. Correlation between device performance and alkyl chain length for NDI-DTYM2 derivatives (**1**−**5**), where the average electron mobility acts as a function of carbon atom number of 2-branched N-alkyl chain (from 12 to 24).

N-alkyl substituents on device performance for NDI-DTYM2 derivatives (**1**−**5**), where the average electron mobility ($\mu_{e,av}$) acts as functions of carbon atom number (N_C, from 12 to 24) of N-alkyl chain. As shown in Figure 9, the chain length affects the device performance, but the effects vary with the annealing temperatures. For the optimum device performance, **2** (N_C = 20) presented the highest average electron mobility of up to 0.32 cm^2 V^{-1} s^{-1},[22] while **1** (N_C = 24) afforded the lowest average mobility of 0.15 cm^2 V^{-1} s^{-1},[22] and **3**−**5** (N_C = 16, 14, and 12, respectively) exhibited the comparable average mobility values of 0.17−0.20 cm^2 V^{-1} s^{-1}. When annealed at 120 °C, thin films of **1**−**5** exhibited comparable average μ_e values approximating 0.10 cm^2 V^{-1} s^{-1}. Higher annealing temperatures (160 and 180 °C) were found to have more positive effects on device performance of **2** (N_C = 20) versus those of **1** and **3**−**5**. When subjected to annealing temperatures ranging from 120 (through 160) to 180 °C, the electron mobility of devices based on **2**−**5** (N_C = 20, 16, 14, and 12, respectively) shows a stepwise improvement and yields the largest $\mu_{e,av}$ values when annealed at 180 °C. However, compound **1** (N_C = 24) presented the optimum device performance ($\mu_{e,av}$ = 0.15 cm^2 V^{-1} s^{-1}) when annealed at 160 °C, and the further annealing at 180 °C yielded a slightly lower $\mu_{e,av}$ value (0.14 cm^2 V^{-1} s^{-1}).[22]

NDI-DTYM2 derivatives **3**, **6**, and **7**, which possess the 2-, 3-, and 4-branched N-alkyl chains of $C_{10,6}$, $C_{11,6}$, and $C_{12,6}$, respectively, with the comparable carbon atom numbers of 16−18, were studied for the structure−property correlations. As shown in Table 2, the device performance of **6** is generally higher than that of **3**, with their optimum average electron mobility of 0.24 and 0.17 cm^2 V^{-1} s^{-1}, respectively. But devices made from **7** exhibited very low electron mobilities of about 10^{-3}−10^{-2} cm^2 V^{-1} s^{-1}, which are lower by 1−2 orders of magnitude versus those of devices based on **3** and **6**. Therefore, the distance of the branching point of the N-alkyl substituent from the NDI core significantly affects the device performance of NDI-DTYM2 derivatives. But what causes the much inferior device performance of **7**? This might be explained by the discontinuous film morphology of **7** to some extent. But the film morphology is not the main reason, because **6** and **7**, having the comparable film morphology when annealed at 180 °C (see Supporting Information Figure S14c,f for details), exhibited distinct device performance ($\mu_{e,av}$: 0.18 versus 0.002 cm^2 V^{-1} s^{-1}). The significant blue shifts (about 18 nm) of thin films of **7** upon annealing, which are different from the slight red-shifts (2−5 nm) for thin films of **3** and **6**, indicate a transition of molecular packing in the films of **7** that works against charge transport and makes the device performance of annealed films even lower than that of the as-deposited films. The detrimental molecular packing, the less-ordered film microstructures, and the discontinuous film morphologies were all responsible for the inferior device performance of **7**.

OTFT devices based on NDI-DTYM2 (**1**−**6**) exhibited high electron mobilities ($\mu_{e,max} \geq$ 0.19 cm^2 V^{-1} s^{-1}) that are orders of magnitude larger than those of devices made form NDI-DTDCN2 (**8** and **9**), NDI-DTYCA2 (**10** and **11**), and NDI-DCT2 (**12**). Since four families of semiconductors have the similar N-alkyl chains, the structurally different π-conjugated backbones might explain their diverse thin-film morphologies and the distinct device performance. DFT calculations reveal a linear, rigid, entirely coplanar and symmetrical π-conjugated backbone for NDI-DTYM2 derivatives. The strong π−π interactions between these perfect π-cores and the hydrophobic interactions between the long 2-branched N-alkyl chains could present a balance that contributes to the good film formation and the resulting high device performance. The inferior device performance ($\mu_e \leq$ 0.016 cm^2 V^{-1} s^{-1}) of NDI-DTDCN2 (**8** and **9**) is probably attributed to the disordered π-conjugated backbone that hinders the densely packing of π-conjugations and results in less efficient charge transport. The aforementioned studies on molecular electron structures demonstrate that NDI-DTYCA2 (**10** and **11**) and NDI-DTYM2 (**1**−**7**) have the identical absorption spectra, comparable LUMO energies (−4.20 eV versus −4.35 eV) and band gap values (2.0 eV versus 2.1 eV), and entirely coplanar and rigid π-conjugated backbones. However, NDI-DTYCA2 (**10** and **11**) exhibited much inferior device performance ($\mu_e \leq 4 \times 10^{-3}$ cm^2 V^{-1} s^{-1}) versus NDI-DTYM2 (**1**−**6**). For NDI-DTYCA2 (**10** and **11**), the protrudent alkoxyl chains attached to the

π-conjugated backbones might be negative factors for the film-forming property and the device performance due to the steric hindrance. The small π-conjugated backbone of NDI-DCT2 (**12**) might lead to its weaker intermolecular interactions in solid state as evidenced by its low melting point (about 160 °C). The weak intermolecular interactions and the poor thin-film morphology might elucidate the inferior device performance of **12** ($\mu_e = 10^{-4}$−10^{-3} cm^2 V^{-1} s^{-1}).

CONCLUSION

This contribution describes a full account of the syntheses, characterizations, and molecular/thin-film properties of four families of core-expanded naphthalene diimides: NDI-DTYM2 (**1**−**7**), NDI-DTDCN2 (**8** and **9**), NDI-DTYCA2 (**10** and **11**), and NDI-DCT2 (**12**). Compounds **1**−**12** are typical n-type organic semiconductors with the low-lying LUMO energies < −4.2 eV. Solution-processed OTFT devices based on **1**−**12** all operated well in air as n-channel transistors. Besides the excellent operating and air stability, OTFT devices based on NDI-DTYM2 (**1**−**6**) exhibited high device performance, with the maximum electron mobilities ≥ 0.19 cm^2 V^{-1} s^{-1}, current on/off ratios > 10^5, and threshold voltages < 15 V. However, NDI-DTDCN2 (**8** and **9**), NDI-DTYCA2 (**10** and **11**), and NDI-DCT2 (**12**) exhibited much inferior device performance, with the maximum electron mobilities of 0.016, 4×10^{-3}, and 1.2×10^{-3} cm^2 V^{-1} s^{-1}, respectively. The studies on the present materials and their OTFT devices demonstrate that both the nature of the branched N-alkyl substituent (the chain length and the position of the branching point) and the π-backbone structure have an impact on the device performance, which implies that the new, solution-processable, high-performance materials could be achieved by fine-tuning the structure of the N-substituent and/or that of the π-backbone. All the results demonstrate that these core-expanded naphthalene diimides fused with sulfur heterocycles and end-capped with electron-withdrawing groups are promising candidates for low-cost, large-area organic electronics.

ASSOCIATED CONTENT

Supporting Information. General experimental methods, synthesis, and characterizations of compounds **3**−**12** and their OTFT devices (PDF). This material is available free of charge via the Internet at http://pubs.acs.org.

AUTHOR INFORMATION

Corresponding Author
*E-mail: gaoxk@mail.sioc.ac.cn; dicha@iccas.ac.cn.

ACKNOWLEDGMENT

The present research was financially supported by Shanghai Natural Science Foundation (09ZR1438500), National Natural Science Foundation (20902105 and 60901050), and the Chinese Academy of Sciences. We thank Prof. Z. G. Shuai for help with DFT calculations.

REFERENCES

(1) For recent reviews on this topic, see: (a) Arias, A. C.; MacKenzie, J. D.; McCulloch, I.; Rivnay, J.; Salleo, A. *Chem. Rev.* **2010**, *110*, 3. (b) Klauk, H. *Chem. Soc. Rev.* **2010**, *39*, 2643. (c) Rogers, J. A.; Someya, T.; Huang, Y. *Science* **2010**, *327*, 1603. (d) Gelinck, G.; Heremans, P.; Nomoto, K.; Anthopoulos, T. D. *Adv. Mater.* **2010**, *22*, 3778.

(2) (a) Gelinck, G. H.; Huitema, H. E. A.; Van Veenendaal, E.; Cantatore, E.; Schrijnemakers, L.; Van der Putten, J. B. P. H.; Geuns, T. C. T.; Beenhakkers, M.; Giesbers, J. B.; Huisman, B.-H.; Meijer, E. J.; Benito, E. M.; Touwslager, F. J.; Marsman, A. W.; Van Rens, B. J. E.; de Leeuw, D. M. *Nat. Mater.* **2004**, *3*, 106. (b) Subramanian, V.; Fréchet, J. M. J.; Chang, P. C.; Huang, D. C.; Lee, J. B.; Molesa, S. E.; Murphy, A. R.; Redinger, D. R.; Volkman, S. K. *Proc. IEEE* **2005**, *93*, 1330. (c) Roberts, M. E.; Sokolov, A. N.; Bao, Z. *J. Mater. Chem.* **2009**, *19*, 3351.

(3) (a) Newman, C. R.; Frisbie, C. D.; da Silva Filho, D. A.; Brédas, J.-L.; Ewbank, P .C.; Mann, K. R. *Chem. Mater.* **2004**, *16*, 4436. (b) Chua, L.-L.; Zaumseil, J.; Chang, J.-F.; Ou, E. C.-W.; Ho, P. K.-H.; Sirringhaus, H.; Friend, R. H. *Nature* **2005**, *434*, 194. (c) Facchetti, A. *Mater. Today* **2007**, *10*, 28. (d) Murphy, A. R.; Fréchet, J. M. J. *Chem. Rev.* **2007**, *107*, 1066.

(4) (a) Crone, B.; Dodabalapur, A.; Lin, Y.-Y.; Filas, R. W.; Bao, Z.; LaDuca, A.; Sarpeshkar, R.; Katz, H. E.; Li, W. *Nature* **2000**, *403*, 521. (b) Meijer, E. J.; De Leeuw, D. M.; Setayesh, S.; Van Veenendaal, E.; Huisman, B.-H.; Blom, P .W. M.; Hummelen, J. C.; Scherf, U.; Klapwijk, T. M. *Nat. Mater.* **2003**, *2*, 678. (c) Klauk, H.; Zschieschang, U.; Pflaum, J.; Halik, M. *Nature* **2007**, *445*, 745.

(5) (a) Bao, Z. *Adv. Mater.* **2000**, *12*, 227. (b) Sirringhaus, H.; Kawase, T.; Friend, R. H.; Shimoda, T.; Inbasekaran, M.; Wu, W.; Woo, E. P. *Science* **2000**, *290*, 2123. (c) Pisula, W.; Menon, A.; Stepputat, M.; Lieberwirth, I.; Kolb, U.; Tracz, A.; Sirringhaus, H.; Pakula, T.; Müllen, K. *Adv. Mater.* **2005**, *17*, 684. (d) Sirringhaus, H. *Adv. Mater.* **2005**, *17*, 2411. (e) Allard, S.; Forster, M.; Souharce, B.; Thiem, H.; Scherf, U. *Angew. Chem., Int. Ed.* **2008**, *47*, 4070.

(6) (a) Payne, M. M.; Parkin, S. R.; Anthony, J. E.; Kuo, C.-C.; Jackson, T. N. *J. Am. Chem. Soc.* **2005**, *127*, 4986. (b) Ebata, H.; Izawa, T.; Miyazaki, E.; Takimiya, K.; Ikeda, M.; Kuwabara, H.; Yui, T. *J. Am. Chem. Soc.* **2007**, *129*, 15732. (c) Subramanian, S.; Park, S. K.; Parkin, S. R.; Podzorov, V.; Jackson, T. N.; Anthony, J. E. *J. Am. Chem. Soc.* **2008**, *130*, 2706. (d) Gao, P.; Beckmann, D.; Tsao, H. N.; Feng, X.; Enkelmann, V.; Baumgarten, M.; Pisula, W.; Müllen, K. *Adv. Mater.* **2009**, *21*, 213. (e) Zhang, W.; Smith, J.; Watkins, S. E.; Gysel, R.; McGehee, M.; Salleo, A.; Kirkpatrick, J.; Ashraf, S.; Anthopoulos, T.; Heeney, M.; McCulloch, I. *J. Am. Chem. Soc.* **2010**, *132*, 11437.

(7) (a) Letizia, J. A.; Cronin, S.; Ortiz, R. P.; Facchetti, A.; Ratner, M. A.; Marks, T. J. *Chem.—Eur. J.* **2010**, *16*, 1911. (b) Ortiz, R. P.; Herrera, H.; Blanco, R.; Huang, H.; Facchetti, A.; Marks, T. J.; Zheng, Y.; Segura, J. L. *J. Am. Chem. Soc.* **2010**, *132*, 8440. (c) Suzuki, Y.; Miyazaki, E.; Takimiya, K. *J. Am. Chem. Soc.* **2010**, *132*, 10453.

(8) Katz, H. E.; Lovinger, A. J.; Johnson, J.; Kloc, C.; Siegrist, T.; Li, W.; Lin, Y.-Y.; Dodabalapur, A. *Nature* **2000**, *404*, 478.

(9) Katz, H. E.; Johnson, J.; Lovinger, A. J.; Li, W. *J. Am. Chem. Soc.* **2000**, *122*, 7787.

(10) (a) See, K. C.; Landis, C.; Sarjeant, A.; Katz, H. E. *Chem. Mater.* **2008**, *20*, 3609. (b) Jung, B. J.; Sun, J.; Lee, T.; Sarjeant, A.; Katz, H. E. *Chem. Mater.* **2009**, *21*, 94. (c) Oh, J. H.; Suraru, S.-L.; Lee, W.-Y.; Könemann, M.; Höffken, H. W.; Röger, C.; Schmidt, R.; Chung, Y.; Chen, W.-C.; Würthner, F.; Bao, Z. *Adv. Funct. Mater.* **2010**, *20*, 2148. (d) Jung, B. J.; Lee, K.; Sun, J.; Andreou, A. G.; Katz, H. E. *Adv. Funct. Mater.* **2010**, *20*, 2930.

(11) (a) Chen, H. Z.; Ling, M. M.; Mo, X.; Shi, M. M.; Wang, M.; Bao, Z. *Chem. Mater.* **2007**, *19*, 816. (b) Li, Y.; Tan, L.; Wang, Z.; Qian, H.; Shi, Y.; Hu, W. *Org. Lett.* **2008**, *10*, 529. (c) Schmidt, R.; Oh, J. H.; Sun, Y.-S.; Deppisch, M.; Krause, A.-M.; Radacki, K.; Braunschweig, H.; Könemann, M.; Erk, P.; Bao, Z.; Würthner, F. *J. Am. Chem. Soc.* **2009**, *131*, 6215.

(12) Zheng, Q.; Huang, J.; Sarjeant, A.; Katz, H. E. *J. Am. Chem. Soc.* **2008**, *130*, 14410.

(13) (a) Yoon, M.-H.; DiBenedetto, S. A.; Facchetti, A.; Marks, T. J. *J. Am. Chem. Soc.* **2005**, *127*, 1348. (b) Di, C.; Li, J.; Yu, G.; Xiao, Y.; Guo, Y.; Liu, Y.; Qian, X.; Zhu, D. *Org. Lett.* **2008**, *10*, 3025.

(14) Wang, Z.; Kim, C.; Facchetti, A.; Marks, T. J. *J. Am. Chem. Soc.* **2007**, *129*, 13362.
(15) (a) Yoo, B.; Jones, B. A.; Basu, D.; Fine, D.; Jung, T.; Mohapatra, S.; Facchetti, A.; Dimmler, K.; Wasielewski, M. R.; Marks, T. J.; Dodabalapur, A. *Adv. Mater.* **2007**, *19*, 4028. (b) Yan, H.; Zheng, Y.; Blache, R.; Newman, C.; Lu, S.; Woerle, J.; Facchetti, A. *Adv. Mater.* **2008**, *20*, 3393.
(16) (a) Jones, B. A.; Ahrens, M. J.; Yoon, M.-H.; Facchetti, A.; Marks, T. J.; Wasielewski, M. R. *Angew. Chem., Int. Ed.* **2004**, *43*, 6363. (b) Piliego, C.; Jarzab, D.; Gigli, G.; Chen, Z.; Facchetti, A.; Loi, M. A. *Adv. Mater.* **2009**, *21*, 1573.
(17) Jones, B. A.; Facchetti, A.; Wasielewski, M. R.; Marks, T. J. *J. Am. Chem. Soc.* **2007**, *129*, 15259.
(18) Handa, S.; Miyazaki, E.; Takimiya, K.; Kunugi, Y. *J. Am. Chem. Soc.* **2007**, *129*, 11684.
(19) Usta, H.; Risko, C.; Wang, Z.; Huang, H.; Deliomeroglu, M. K.; Zhukhovitskiy, A.; Facchetti, A.; Marks, T. J. *J. Am. Chem. Soc.* **2009**, *131*, 5586.
(20) (a) Yan, H.; Chen, Z.; Zheng, Y.; Newman, C.; Quinn, J. R.; Dötz, F.; Kastler, M.; Facchetti, A. *Nature* **2009**, *457*, 679. (b) Chen, Z.; Zheng, Y.; Yan, H.; Facchetti, A. *J. Am. Chem. Soc.* **2009**, *131*, 8. (c) Baeg, K.-J.; Khim, D.; Kim, D.-Y.; Jung, S.-W.; Koo, J. B.; You, I.-K.; Yan, H.; Facchetti, A.; Noh, Y.-Y. *J. Polym. Sci., Polym. Phys.* **2011**, *49*, 62.
(21) (a) Tang, M. L.; Oh, J. H.; Reichardt, A. D.; Bao, Z. *J. Am. Chem. Soc.* **2009**, *131*, 3733. (b) Wen, Y.; Liu, Y. *Adv. Mater.* **2010**, *22*, 1331. (c) Delgado, M. C. R.; Kim, E.-G.; da Silva Filho, D. A.; Brédas, J.-L. *J. Am. Chem. Soc.* **2010**, *132*, 3375. (d) Sakai, N.; Mareda, J.; Vauthey, E.; Matile, S. *Chem. Commun.* **2010**, *46*, 4225. (e) Tang, Q.; Liang, Z.; Liu, J.; Xu, J.; Miao, Q. *Chem. Commun.* **2010**, *46*, 2977.
(22) Gao, X.; Di, C.; Hu, Y.; Yang, X.; Fan, H.; Zhang, F.; Liu, Y.; Li, H.; Zhu, D. *J. Am. Chem. Soc.* **2010**, *132*, 3697.
(23) Yamashita, Y.; Suzuki, T.; Saito, G.; Mukai, T. *J. Chem. Soc., Chem. Commun.* **1986**, 1489.
(24) (a) Kastler, M.; Pisula, W.; Wasserfallen, D.; Pakula, T.; Müllen, K. *J. Am. Chem. Soc.* **2005**, *127*, 4286. (b) Balakrishnan, K.; Datar, A.; Naddo, T.; Huang, J.; Oitker, R.; Yen, M.; Zhao, J.; Zang, L. *J. Am. Chem. Soc.* **2006**, *128*, 7390. (c) Wicklein, A.; Lang, A.; Muth, M.; Thelakkat, M. *J. Am. Chem. Soc.* **2009**, *131*, 14442. (d) Vaidyanathan, S.; Dötz, F.; Katz, H. E.; Lawrentz, U.; Granstrom, J.; Reichmanis, E. *Chem. Mater.* **2007**, *19*, 4676. (e) Kreyes, A.; Ellinger, S.; Landfester, K.; Defaux, M.; Ivanov, D. A.; Elschner, A.; Meyer-Friedrichsen, T.; Ziener, U. *Chem. Mater.* **2010**, *22*, 2079.
(25) Gao, X.; Qiu, W.; Yang, X.; Liu, Y.; Wang, Y.; Zhang, H.; Qi, T.; Liu, Y.; Lu, K.; Du, C.; Shuai, Z.; Yu, G.; Zhu, D. *Org. Lett.* **2007**, *9*, 3917.
(26) Matsuoka, M.; Iwamoto, A.; Kitao, T. *J. Heterocyclic Chem.* **1991**, *28*, 1445.
(27) (a) Laquindanum, J. G.; Katz, H. E.; Lovinger, A. J. *J. Am. Chem. Soc.* **1998**, *120*, 664. (b) Payne, M. M.; Odom, S. A.; Parkin, S. R.; Anthony, J. E. *Org. Lett.* **2004**, *6*, 3325. (c) Anthony, J. E.; Subramanian, S.; Parkin, S. R.; Park, S. K.; Jackson, T. N. *J. Mater. Chem.* **2009**, *19*, 7984.
(28) Kwon, O.; Coropceanu, V.; Gruhn, N. E.; Durivage, J. C.; Laquindanum, J. G.; Katz, H. E.; Cornil, J.; Brédas, J. L. *J. Chem. Phys.* **2004**, *120*, 8186.
(29) (a) de Leeuw, D. M.; Simenon, M. M. J.; Brown, A. R.; Einerhand, R. E. F. *Synth. Met.* **1997**, *87*, 53. (b) Usta, H.; Facchetti, A.; Marks, T. J. *J. Am. Chem. Soc.* **2008**, *130*, 8580.
(30) Anthopoulos, T. D.; Anyfantis, G. C.; Papavassiliou, G. C.; de Leeuw, D. M. *Appl. Phys. Lett.* **2007**, *90*, 122105.
(31) (a) Weitz, R. T.; Amsharov, K.; Zschieschang, U.; Villas, E. B.; Goswami, D. K.; Burghard, M.; Dosch, H.; Jansen, M.; Kern, K.; Klauk, H. *J. Am. Chem. Soc.* **2008**, *130*, 4637. (b) Sirringhaus, H. *Adv. Mater.* **2009**, *21*, 3859. (c) Oh, J. H.; Sun, Y.-S.; Schmidt, R.; Toney, M . F.; Nordlund, D.; Könemann, M.; Würthner, F.; Bao, Z. *Chem. Mater.* **2009**, *21*, 5508.
(32) (a) Ling, M.-M.; Erk, P.; Gomez, M.; Koenemann, M.; Locklin, J.; Bao, Z. *Adv. Mater.* **2007**, *19*, 1123. (b) Weitz, R. T.; Amsharov, K.; Zschieschang, U.; Burghard, M.; Jansen, M.; Kelsch, M.; Rhamati, B.; van Aken, P. A.; Kern, K.; Klauk, H. *Chem. Mater.* **2009**, *21*, 4949.
(33) Osaka, I.; Zhang, R.; Sauvé, G.; Smilgies, D.-M.; Kowalewski, T.; McCullough, R. D. *J. Am. Chem. Soc.* **2009**, *131*, 2521.
(34) Single crystal X-ray analysis is a good way to understand the molecular array and the resulting charge transport behavior in solid state. Unfortunately, we failed to obtain suitable single crystals for present materials, due to their long branched N-alkyl substituents that work against the single crystal growth. Synthesis of model compounds that can form suitable single crystals and characterization of thin films of the present materials using the grazing incidence X-ray diffraction (GIXD) are underway for an in-depth understanding of structure−function relationships.